Phonon coherent transport leads to an anomalous boundary effect on the thermal conductivity of a rough graphene nanoribbon

Shuang Tian,[1] Tingting Wang,[1] Hao Chen,[2,*] Dengke Ma,[1,†] and Lifa Zhang[1]

[1] *Phonon Engineering Research Center of Jiangsu Province, Center for Quantum Transport and Thermal Energy Science, Institute of Physics Frontiers and Interdisciplinary Sciences, School of Physics and Technology, Nanjing Normal University, Nanjing 210023, China*

[2] *Department of Physics, University of Science and Technology of China, Hefei 230026, China*

(Received 19 September 2023; revised 18 April 2024; accepted 14 May 2024; published 4 June 2024; corrected 17 June 2024)

Coherent phonons can give rise to phenomena and physical mechanisms in different systems. Understanding phonon-boundary scattering is critical for the manipulation of thermal properties. In this paper, it is found that the thermal conductivity of rough graphene nanoribbon first monotonically changes, and then exhibits an oscillatory manner with the varying of surface boundary roughness. An obvious increase in thermal conductivity, up to 25.33%, can be observed as surface boundary roughness increases from 0.61 to 0.72. This is in contrast to the conventional understanding that thermal conductivity typically decreases when surface boundary roughness increases. Further, a frequency-resolved picture and lattice dynamics analysis identify that the anomalous boundary effect originates from the coherent nature of phonons, which results in the roughness-selected destructive interference of different modes. Besides, the oscillation will be reduced by introducing rough boundaries with different sinusoidal shapes, which increases the randomness. This abnormal boundary effect can also be extended to other materials, for example, hexagonal boron nitride monolayer, depending mainly on the anharmonicity. The study reveals physical insights into phonon-boundary scattering and may aid the design of heat management and thermoelectric devices based on the boundary effect.

DOI: 10.1103/PhysRevApplied.21.064005

I. INTRODUCTION

Boundary effects play significant roles in many fields, varying from chemical reaction dynamics [1], gene regulations [2], to especially condensed-matter physics [3–5]. Many physical properties of materials, for example, giant magnetoresistance of an Fe/Cr superlattice [6], spin-stripe correlation in superconductors [3], hydrodynamic flow of electron fluid [4], and photovoltaic properties of thin-film perovskites [5], can be modulated by changing boundary morphology or conditions. In the area of thermal science, phonon-boundary scattering is considered as one of the basic mechanisms to tailor thermal properties of materials, which has been widely adopted to facilitate heat dissipation by enhancing interfacial thermal conductance [7,8] and optimize energy conversion of thermoelectric by decreasing lattice thermal conductivity [9–12].

Considering the boundary effect on phonons, the wave (coherent) and particle (incoherent) nature will govern phonon transport in different behaviors and mechanisms [13,14]. As revealed by previous works, phonon coherent transport impacts thermal conductivities via interference, which is quite different from incoherent phonons [15–18]. Several physical mechanisms induced by phonon coherent transport have been found in different systems, for example, phonon resonance hybridization in pillared structures, which blocks phonon transport and is not expected to scatter electrons [15,19], phonon localization in disordered superlattices, which results in the nonmonotonic dependence of thermal conductivity on system length [16,20,21], and mutual coherence among different phonon branches in highly anharmonic or complex materials [17,22,23]. The above findings all enrich our fundamental understanding of phonons and provide guidance for further phonon engineering and tailoring of thermal properties [10,24].

Theoretical and experimental studies reveal that phonon-surface boundary scattering blocks phonon transport, and by increasing surface-boundary roughness, thermal conductivity can be further decreased [9,25–29]. Considering the coherent nature of phonons, interference depends on both the wavelength of phonons and the characteristic structure size [30,31]. So, it is possible that a system with larger surface-boundary roughness can induce less destructive interference. When coherent transport dominates, a larger thermal conductivity may be realized

*Corresponding author: phych@njnu.edu.cn
†Corresponding author: dkma@njnu.edu.cn

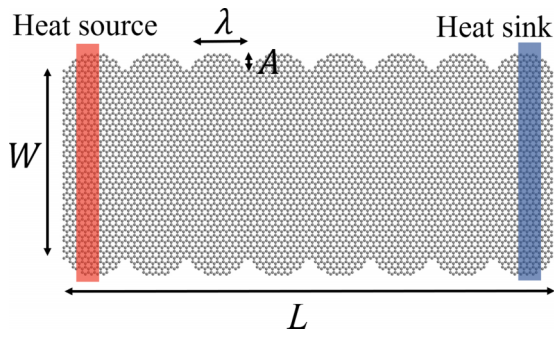

FIG. 1. Schematic picture of RGNR, which is made by tailoring two boundaries of GNR with the same sinusoidal curve. The λ and W is set as 2.49 and 5 nm, respectively.

on a system with larger roughness. A simulation study by a simple Lorentz gas model reported the nonmonotonic dependence of thermal conductivity on surface-boundary roughness [32]. However, the system is considered as an idea continuum harmonic media, adopting a gray heat carrier model, which does not consider phonon dispersion. Real materials all have nonlinearity, which plays a significant role in thermal transport [33], and consists of discrete atoms. Particularly, phonons have different wave vectors, frequencies, polarization, and wavelength, which have different contributions to thermal conductivity [23,33]. Can the nonmonotonic dependence of thermal conductivity on surface-boundary roughness be found in real materials? What are the underlying mechanism and spectral features?

In the paper, the thermal conductivity of rough graphene nanoribbons (RGNR, shown in Fig. 1, κ_{RGNR}) is studied by nonequilibrium molecular dynamics (NEMD) simulation. Another two-stage dependence of κ_{RGNR} on surface-boundary roughness is found on RGNR. Including the parameter studies by changing the system length (L), width (W), temperature (T_0), and randomness of sinusoidal shapes, the underlying mechanism of the anomalous dependence of κ_{RGNR} on surface-boundary roughness is clarified by means of lattice dynamics and a frequency-resolved picture, and this mechanism is mainly dependent on material anharmonicity.

II. METHOD

The configuration of RGNR is achieved by tailoring two boundaries of GNR with the same sinusoidal curve, which is shown in Fig. 1. This structure can be synthesized with atomic precision through the bottom-up approach in experiment [34,35]. For this system, the boundary roughness is defined as $u = A/\lambda$, where A and λ are the amplitude and half-period of the sinusoidal curve, respectively (shown in Fig. 1). To keep λ the same in the following discussions for a system with specific length, the roughness is changed by adjusting A. Wave interference occurs when the characteristic length is comparable to the phonon wavelength. As we focus on the temperature above 200 K where the phonon wavelength is small and about several nanometers. So, a value of 2.49 nm is set for λ. When temperature decreases, the characteristic length can be longer at about tens of nanometers. Then, the value of λ is comparable to experimental results. This is because low-frequency phonons dominate thermal transport at low temperature, which generally have long wavelengths. The lattice constant of RGNR is 0.1438 nm and the thickness (d) is 0.335 nm.

It needs to be noticed that the displayed RGNR in Fig. 1 is its initial input morphology, which seems to have regular sinusoidal shapes and there is no randomness of surface boundaries. Here, to investigate the surface boundary's effect, the free-boundary condition is adopted. This is the commonly used strategy to investigate surface effect, as can be seen in various previous studies [36,37]. After structure relaxation, randomness will be naturally introduced by morphology reconstruction. That is, atoms at each sinusoidal shape will deviate from their initial positions randomly. Thus, each sinusoidal shape is different and can be treated as rough boundaries (a detailed discussion can be found in Part I within the Supplemental Material [38]).

NEMD simulations are performed using the LAMMPS package [39], and optimized Tersoff potential is adopted to describe interactions among atoms [40]. We should also notice that Simoncelli *et al*. and different researches proposed theoretical models to describe the phonon coherent effect by introducing an extra term of the off-diagonal part of the Wigner operator [17,22,23,41]. To calculate the contribution of the off-diagonal part (coherent effect) to thermal conductivity, different phonon information needs to get through first-principles calculation [17,41]. Due to the computational cost, the present studies adopting the theories are mainly focused on perfect crystal with simulated supercell containing tens, at most up to one or two hundred atoms. As MD simulation implicitly includes the phonon coherent and incoherent nature, it is a good choice to study the coherent phonon effect on nanostructures [15,16].

The free- and fixed-boundary conditions are applied in the transverse and longitudinal directions, respectively. To establish a temperature gradient (∇T), the system is connected to the Langevin thermostats at the 5th to 12th and (N-12)th to (N-5)th layer (1.0 nm). Temperatures are $T_R = T_0\,(1 + \Delta)$ and $T_L = T_0\,(1 - \Delta)$, respectively, where T_0 is the average temperature and Δ is the temperature difference. Further simulation details about the effect of the heat source can be found in Part II within the Supplemental Material [38]. The velocity Verlet method is used to integrate Newton's equation of motion with a timestep of 0.5 fs. Initially, the system is relaxed in the isothermal-isobaric ensemble (NPT) at T_0 and 0 bar for 2×10^6 steps. Then, the system is moved to the microcanonical ensemble (NVE), relaxed for 5×10^6 steps. Finally, the temperature

and heat flux are averaged over 1×10^7 steps under NVE. The results presented in this paper are averaged over six independent simulations with different initial conditions.

The thermal conductivity can be calculated by Fourier's law,

$$\kappa = -\frac{J}{W \cdot d \cdot \nabla T}, \tag{1}$$

where J is the heat flux from the heat source to the heat sink. W and d are the width and thickness of RGNR, respectively. The ∇T is obtained through linear fitting of local temperature, not including the temperature jumps of both ends. It should be noticed that, the amplitude (A) of the rough boundary is not included in W. So, when changing the u, the W stays the same.

III. RESULTS AND DISCUSSION

A. Two-stage behavior of thermal conductivity

The dependence of κ_{RGNR} on surface-boundary roughness for systems with different L is shown in Figs. 2(a) and 2(b) (error bars for all data are shown in Part III within the Supplemental Material [38]). Here, T_0 is 300 K, and W is fixed as 5 nm. It can be observed that, when u increases, κ_{RGNR} shows an anomalous two-stage behavior for all the four systems with different L. At the first stage, κ_{RGNR} monotonically decreases when u increases from 0.17 to 0.43. This is consistent with previous studies that larger surface-boundary roughness induces stronger phonon scattering and decreases thermal conductivity more heavily [9,26,27]. At the second stage, when u is larger than 0.43, κ_{RGNR} shows an oscillatory manner. Particularly, when u increases from 0.61 to 0.72, κ_{RGNR} exhibits a striking increase [as shown in Fig. 2(b)]. For example, κ_{RGNR} increases from 240.45 to 284.64 W m^{-1} K^{-1} for the system with L equal to 100 nm. At the same time, it can be found that the oscillation of κ_{RGNR} at the second stage becomes stronger when L increases (details explained later). This can be obviously observed on the normalized κ_{RGNR}, which is shown in Fig. S4(a) within the Supplemental Material [38]. To quantitatively show this point, we focus on the increase ratio of κ_{RGNR} when u changes from 0.61 to 0.72. For systems with L equal to 40, 70, 100, and 130 nm, the increase ratios are 10.65%, 11.16%, 18.38%, and 13.44%, respectively. Noting that in the whole roughness range, κ_{RGNR} is larger for systems with longer L. This is due to the size-dependent thermal conductivity, which has been widely studied previously [42]. The dependence of κ_{RGNR} on surface-boundary roughness for systems with different W is provided in Part V within the Supplemental Material [38].

Changing T_0 will also alter the roughness dependence of κ_{RGNR}, which is shown in Fig. 2(c). Here, L and W are fixed as 100 and 5 nm, respectively. It can be observed

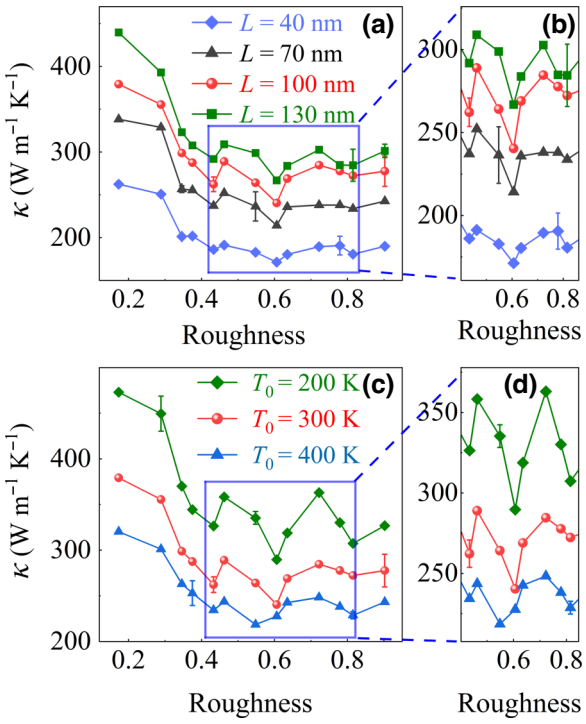

FIG. 2. Thermal conductivity of RGNR for systems with different (a) length and (c) temperature as a function of surface-boundary roughness. (b),(d) are picked from (a),(c), respectively, which focus on the oscillatory region.

that the increase of T_0 weakens the oscillation of κ_{RGNR} at the second stage (see the normalized κ_{RGNR} in Fig. S4(b) within the Supplemental Material [38]). The increase ratios of κ_{RGNR}, by comparing systems with u changes from 0.61 to 0.72, are 25.33%, 18.38%, and 8.85% (13.47% for u changes from 0.55 to 0.72) when T_0 is equal to 200, 300, and 400 K, respectively. This weakening of oscillation originates from the breaking of phonon coherence with the increase of T_0, which will be explained in detail later. Noting that in the whole roughness range, κ_{RGNR} decreases when T_0 increases. This is due to the Umklapp multiphonon scattering, which is strengthened as T_0 increases [33,43].

B. Behind mechanism of roughness-selected destructive interference of different modes

To clarify the underlying mechanism, vibration eigenmode analysis of phonons in RGNR for systems with different u is carried out through the general utility lattice program (GULP) [44] using the same potential as NEMD simulation. The participation ratio (PR) for each mode (focused on u is equal to 0.61 and 0.72), which can quantitatively measure the spread out of mode [45,46], is calculated and shown in Fig. 3(a) (calculation details are provided in Part VI within the Supplemental Material [38]). It can be found that for RGNR with smaller

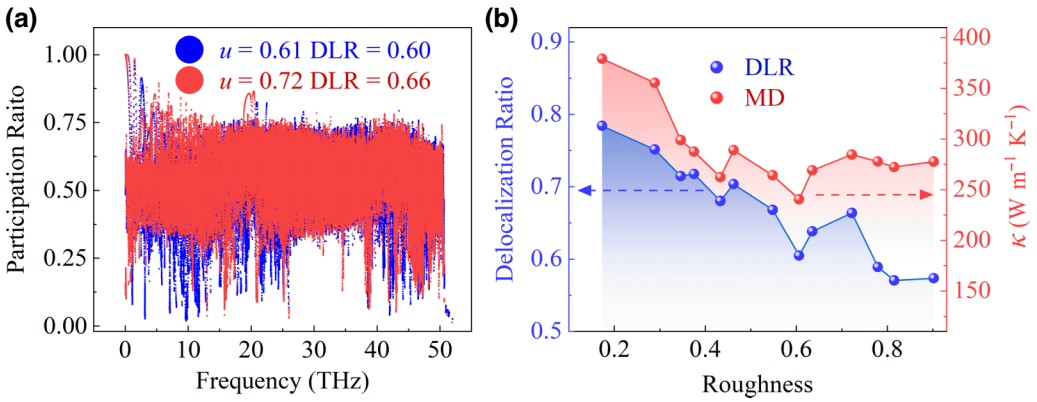

FIG. 3. (a) The PR for RGNR with u equal to 0.61 (blue dot) and 0.72 (red dot). The delocalization ratio (DLR) are calculated according to the definition in the text. (b) The comparison between DLR and thermal conductivity for RGNR with different boundary roughness.

u (0.61, blue dot), phonons have smaller PRs in low and middle frequencies and several high frequencies. It means that many atoms cannot participate in the vibration of these modes (can also be treated as localized modes), which are experienced destructive interference. Thus, thermal conductivity decreases even u is smaller. If we focus on the normal case when u decreases from 0.61 to 0.46. As shown in Fig. S6(a) within the Supplemental Material [38], for RGNR with smaller u (0.46, green dot), phonons have larger PRs in low and middle frequencies. It means that more atoms can participate in the vibration. As a result, these phonons transport well at the system, leading to an enhancement in thermal conductivity when u decreases from 0.61 to 0.46.

It also needs to be noticed that, for RGNR when u is equal to 0.46 and 0.72, although their thermal conductivities are nearly the same (288.98 and 284.64 W m^{-1} K^{-1}), the modes that have smaller PR are different and distributed in different frequencies. As shown in Fig. S6(b) within the Supplemental Material [38], when u is equal to 0.72, modes near 10.5, 15.5, 21, 34.5, and 39 THz have smaller PR. However, when u is equal to 0.46, other modes appear near 19.5 THz, 45 THz and several low frequencies ranging from 4 to 9 THz that have smaller PR. This is because destructive interference is a combined effect, which depends on both roughness and wavelength. Since different modes have different wavelengths [23,30], for RGNR with a different u, modes that experience destructive experience are different. The above point can be figured out more obviously by the nonparticipation ratio, inverse of PR, as shown in Fig. S7 within the Supplemental Material [38].

Understanding the above mechanism of roughness-selected destructive interference, the increase of κ_{RGNR} when u increase is rational. A system with larger u induces destructive interference for fewer phonons. To better show that roughness-selected destructive interference is the underlying mechanism, the delocalization ratio (DLR) is introduced, which is defined as the percentage of numbers of eigenmodes whose PR is larger than 0.5. According to this definition, a larger DLR means less destructive interference, and a larger thermal conductivity. As shown in the inset of Fig. 3(a), the DLR are 0.60 and 0.66 for RGNR when u is equal to 0.61 and 0.72, respectively. This means fewer phonons experience destructive interference when u increases and is equal to 0.72, which results in the larger κ_{RGNR}. More generally, the DLR for RGNR with different u ranging from 0.17 to 0.90 is calculated, and compared with the κ_{RGNR} shown in Fig. 2. As shown in Fig. 3(b), the DLR (blue dot) shares nearly the same trend as κ_{RGNR} calculated by NEMD (red dot). This further demonstrated that roughness-selected destructive interference induced by coherent phonons is the underlying mechanism, which is responsible for the anomalous roughness-dependent κ_{RGNR}, as well as the anomalous boundary effect in RGNR.

To further confirm that destructive interference is induced by rough boundaries, and visualize different modes. The distributions of amplitude for a specific localized mode ($\omega = 1.12$ THz) and spread out mode ($\omega = 20.80$ THz) are projected on the supercell of RGNR and shown in Fig. 4. As all eigenvectors are orthogonally normalized. For localized mode with $\omega = 1.12$ THz, it distributes mainly on the rough boundaries. Atoms at the sinusoidal boundary area have much larger amplitude than those at the inner of the ribbon. That is, phonons transported along the longitudinal direction, which contribute to thermal conductivity, are localized at the boundaries. This will result in the decrease of participation ratio, and the projection of these localized modes is distributed at boundaries. However, for the spread out mode with $\omega = 20.80$ THz, all atoms vibrate with nearly the same amplitude. Atoms at the ends of the sinusoidal boundary have even smaller amplitude than those at the inner of the ribbon. As the sinusoidal boundary areas are not directly contacted, different supercells are connected through the

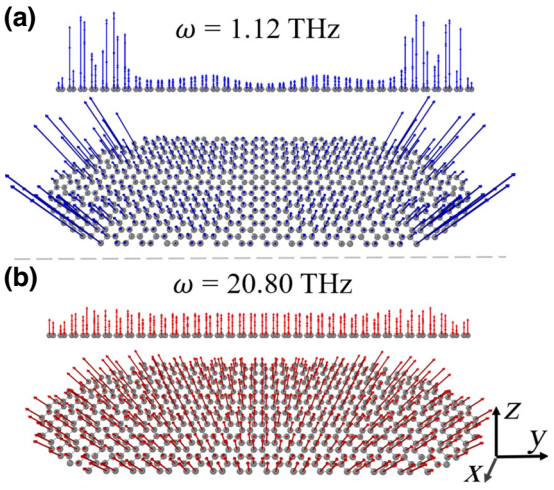

FIG. 4. Comparison and visualization of two eigenmodes with PR equal to 0.16 and 0.80 for RGNR when $u = 0.61$.

inner of the ribbon. The spread out modes can easily propagate along different supercells and contribute to thermal conductivity, while localized modes can hardly be transported. The above picture of phonon localization induced by the surface-boundary effect has been discussed in detail in various previous studies [37,47].

As lattice dynamics analysis presented above considers only the harmonic effect, to take the anharmonic effect into account, the decomposed spectral heat flux is extracted through NEMD by tracking force-velocity correlations among atoms [16,48]. Divided by cross-section area and temperature gradient, the frequency-dependent thermal conductivity can be obtained and is shown in Fig. 5. And the corresponding frequency-dependent thermal conductivity using a linear scale is shown in Fig. S8 of the Supplemental Material [38]. Here, T_0 and L are equal to 200 K and 100 nm, respectively. The spectral

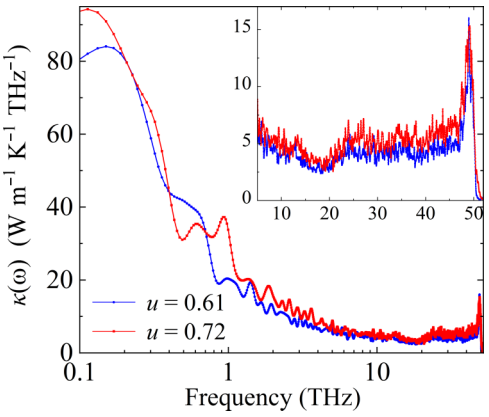

FIG. 5. The frequency-dependent thermal conductivity of RGNR with u equal to 0.61 (blue line) and 0.72 (red line) at 200 K. Inset: focus on a magnification of the frequency between 5 and 52 THz.

κ_{RGNR} for the system with u equal to 0.72 is larger than that with u equal to 0.61 in many frequency ranges, especially for low-frequency modes. This is because low-frequency phonons have longer wavelength, and are more likely to show coherent nature. Thus, the boundary-roughness-selected destructive interference is more obvious at low frequency.

C. Explanation for the length and temperature-dependent thermal conductivity

The temperature and system-length-dependent oscillation in κ_{RGNR} can be understood following the above rationale. When T_0 increases from 200 K, 300 K to 400 K, the increase ratios of κ_{RGNR} when u changes from 0.61 to 0.72 decreases from 25.33% to 18.38% and 8.85%. This is because multiphonon scattering increases [33,43,49] as temperature increases. This destroys the phase information, as well as coherence of phonons. As interference is derived from the coherent nature of phonon. The breaking of coherence will weaken destructive interference, which leads to the anomalous boundary effect here. Thus, the oscillation in κ_{RGNR} weakens.

At the same time, as shown in Fig. 6, the increase ratio of κ obviously increases when L increases from 40 nm, reaching a maximum value of 25.33% and 18.38% at 200 and 300 K, respectively when L reaches 100 nm. However, as L further increases from 100 to 160 nm, a noteworthy decrease in oscillation of κ_{RGNR} is observed. When L increases to 160 nm, the increase ratios gradually decrease to 16.33% and 11.73% for temperatures of 200 and 300 K, respectively. This behavior differs from that observed in the range of 40 to 100 nm. This is because when L is small, more phonons whose velocities are parallel to or deviated from longitudinal direction in a certain degree can be ballistically transported from heat bath to heat sink. That is, they will not reach the surface boundaries,

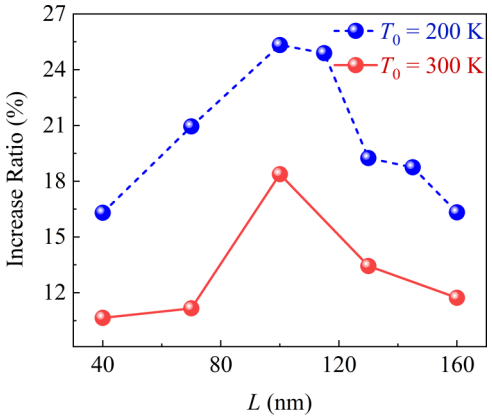

FIG. 6. The dependence of the increase ratio for RGNR on system length at 200 and 300 K, respectively.

and the boundary effect does not work. Under this condition, when L increases, more phonons will collide with rough boundaries, some will even experience multiple collision with boundaries. This will increase the possibility of destructive interference, and strengthen the oscillation in κ_{RGNR}. However, when L further increases and is larger than the mean-free-path of some modes. These modes will experience multiphonon scattering, which will also break coherence. As a result, the oscillation in κ_{RGNR} weakens. Thus, the increase of L brings two competitive mechanisms, which leads to the nonmonotonic change of increase ratio.

D. The effect of randomness induced by the difference of sinusoidal shapes on thermal conductivity

It also needs to be noticed that the randomness discussed above is introduced by morphology reconstruction under free-boundary conditions, which makes atomic locations at each sinusoidal area different. Except that, the randomness induced by the difference of sinusoidal shapes is also a key factor, which may affect the selection of localization modes. To check this point, we introduce randomness to the sinusoidal shape. That is, sinusoidal shape with different amplitude [as shown in Fig. 7(a)], termed as A', is randomly introduced to RGNR to replace the original sinusoidal shape with amplitude equals to A. Here, we focus on the RGNR with L and W of 100 and 5 nm, respectively. T_0 is fixed as 200 K.

Firstly, we focus on the effect of replacement percentage (RP), which is defined as the number of sinusoidal shapes with amplitude equal to A' divided by the total number of sinusoidal shapes. The A' is fixed as 0.72 nm. Taking the sketches of RGNR shown in Fig. 7(a) as an example, there are 14 sinusoidal shapes on each side of RGNR. By keeping the boundaries symmetrical, three sinusoidal shapes on each side are randomly selected and their amplitudes are replaced by A'. The RP is calculated as 21.4%. To investigate the effect of RP on oscillatory of κ_{RGNR}. The κ_{RGNR} is calculated for the structures with the same u of 0.61 and 0.72, where the κ_{RGNR} exhibits a striking increase as shown in Fig. 2. As depicted in Fig. 7(a), the increase ratio decreases as the RP increases. This means that the oscillation in κ_{RGNR} weakens as the sinusoidal shape randomness increases. However, even when RP reaches 37.5%, the κ_{RGNR} increase ratio remains at 11.77%.

Then, the RP is fixed, and we focus on the change of randomness by decreasing A' from 1.5 to 0.0 nm. Similarly, we also focus on the RGNR with the same u of 0.61 and 0.72 (A/λ). As shown in Fig. 7(b), for both the two cases of RP equal to 2.5% and 25%, the increase ratio of κ_{RGNR} decreases as A' decreases. This is because the replaced A' is smaller than A, the randomness increases as A' decreases. When A' is reduced to 0 nm, the increase ratio of κ_{RGNR} is 2.6% for the system with larger RP equal

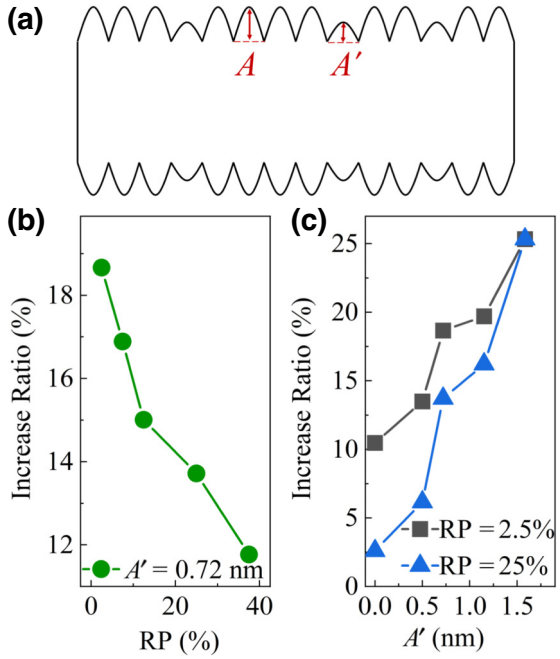

FIG. 7. (a) Sketches of RGNR with sinusoidal shape of different amplitude A', which is randomly introduced. The increase ratio when u changes from 0.61 to 0.72 in the thermal conductivity of RGNR for systems with respect to the (a) replacement proportion and (b) amplitude after introducing randomness.

to 25%. This means the oscillation of κ_{RGNR} in the second stage almost disappears. Thus, we can conclude that the randomness induced by the difference of sinusoidal shapes will weaken the oscillation, which originates from the roughness-selected destructive interference of different modes. This is because it is the characteristic size of sinusoidal shape that selects the modes with certain wavelengths to be localized at the sinusoidal area where atoms are randomly localized. The introduced sinusoidal shape with different characteristic size will be broken in this selection, thus, weakening the oscillation.

E. Extended to other materials

As a final remark, we should emphasize that the anomalous phenomena of two-stage dependence of thermal conductivity on surface-boundary roughness is not only limited to the specific material of the graphene nanoribbon, which would be found on both nanoribbons and nanowires of other materials. Here, an alternative rough graphene nanoribbon is chosen because graphene has weak anharmonicity, and phonons in graphene have a long mean free path and wavelength [10,50]. As revealed here, the behind mechanism is roughness-selected destructive interference for different modes, which originates from the coherent nature of phonons. The anomalous boundary effect is expected to be found on other materials with weak anharmonicity at room temperature [15,50], and even

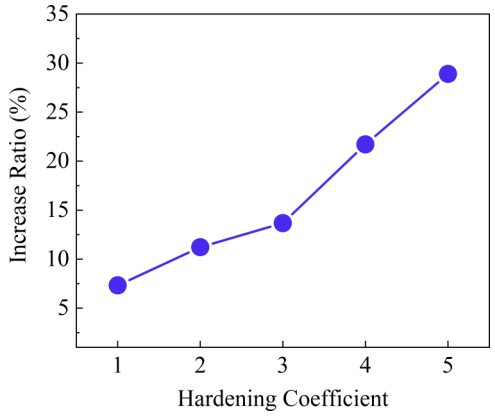

FIG. 8. The dependence of increase ratio for *h*-BN on the hardening coefficient of interatomic bonding force at 200 K.

materials with strong anharmonicity at low temperature where low-frequency phonons dominate thermal transport and generally have long wavelengths [51].

To support the above point, we also investigate the boundary effect on hexagonal boron nitride monolayer (*h*-BN). Adopting the same scenario as RGNR, we tailor two boundaries of *h*-BN with sinusoidal curve, and calculate the dependence of thermal conductivity for rough *h*-BN ($\kappa_{\text{Rh-BN}}$) on surface roughness. The lattice constant of *h*-BN is 0.1449 nm, and its thickness is 0.33 nm. The Tersoff potential is used to describe the interaction between B-B, N-N, and B-N atomic pairs [52]. The NEMD simulation is performed under the same conditions as RGNR. Here T_0 is 200 K, and W and L are fixed at 5 and 100 nm, respectively. The increase ratio is 7.32% for Rh-BN when the surface-roughness increases from 0.61 to 0.72, which is smaller than RGNR. This is because the *h*-BN has a stronger anharmonicity than graphene. To weaken its anharmonicity, we can harden its interatomic bonding force. The dependence of increase ratios of $\kappa_{\text{Rh-BN}}$ on the hardening coefficient of bonding force is shown in Fig. 8. When the hardening coefficient is equal to 1, it corresponds to original *h*-BN. It can be observed that the increase ratio of κ_{RGNR} enhances as the hardening coefficient increases. When the hardening coefficient increases to 5, the increase ratio is up to 28.89%. Thus, we can conclude that the oscillating thermal conductivity can exist for other materials, which mainly depends on the anharmonicity.

IV. CONCLUSIONS

In summary, κ_{RGNR} is investigated by NEMD simulation. The results reveal that the κ_{RGNR} shows an two-stage dependence on surface-boundary roughness. At the first stage, κ_{RGNR} monotonically decreases when u increases. This is consistent with previous studies. At the second stage, κ_{RGNR} shows an oscillatory manner when u increases. Particularly, when u increases from 0.61 to 0.72, κ_{RGNR} exhibits a striking increase. System length and temperature can have large influence on this abnormal u-dependent κ_{RGNR}. After comparatively studying eigenmodes for RGNR with different u by lattice dynamics, it is demonstrated that roughness-selected destructive interference induced by coherent phonons is the underlying mechanism. Introducing rough boundaries with different sinusoidal shapes, which breaks the mode selection, will decrease the oscillation in κ_{RGNR}. Moreover, as this abnormal oscillation behavior of thermal conductivity mainly depends on anharmonicity, and can exist in other materials, for example, a hexagonal boron nitride monolayer. The findings here significantly enrich our fundamental understanding of phonon-boundary scattering and coherent phonon transport.

The rules of two-stage dependence of thermal conductivity on surface-boundary roughness will aid the design of materials for thermoelectrics and heat dissipation, which tie to phonon-boundary scattering. Specifically, to improve the efficiency of thermoelectric materials, increasing surface-boundary roughness to decrease lattice thermal conductivity (such as silicon nanowire) has become a widely adopted strategy [9]. The findings here indicate that continuously increasing surface-boundary roughness will not always work, a minimum thermal conductivity can be achieved by structures with certain roughness, which is related to their phonon properties. This scenario will be the same for heat-dissipation materials with high thermal conductivity, which are generally thought to be benefited from smaller surface-boundary roughness. The roughness of idea structures for heat dissipation is zero, while, this is impossible. Because rough boundaries are inevitable due to the decrease of coordination number for atoms at surfaces and chemical passivation [53]. As a result, choosing structures with certain roughness, which blocks phonon transport to the minimum degree is useful.

ACKNOWLEDGMENTS

This work is sponsored by National Natural Science Foundation of China (Grant No. 12275133) and Department of Science and Technology of Jiangsu Province (Grants No. BK20231279 and No. BK20220032) and Postgraduate Research & Practice Innovation Program of Jiangsu Province (Grant No. KYCX23_1677).

The authors declare that they have no known competing financial interests or personal relationships that could have appeared to influence the work reported in this paper.

[1] R. G. Mariano, K. McKelvey, H. S. White, and M. W. Kanan, Selective increase in CO_2 electroreduction activity

at grain-boundary surface terminations, Science **358**, 1187 (2017).

[2] K. C. Akdemir, V. T. Le, S. Chandran, Y. Li, R. G. Verhaak, R. Beroukhim, P. J. Campbell, L. Chin, J. R. Dixon, P. A. Futreal, P. S. V. W. Group, and P. Consortium, Disruption of chromatin folding domains by somatic genomic rearrangements in human cancer, Nat. Genet. **52**, 294 (2020).

[3] E. W. Huang, C. B. Mendl, S. Liu, S. Johnston, H.-C. Jiang, B. Moritz, and T. P. Devereaux, Numerical evidence of fluctuating stripes in the normal state of high-T_c cuprate superconductors, Science **358**, 1161 (2017).

[4] A. C. Keser, D. Q. Wang, O. Klochan, D. Y. H. Ho, O. A. Tkachenko, V. A. Tkachenko, D. Culcer, S. Adam, I. Farrer, D. A. Ritchie, O. P. Sushkov, and A. R. Hamilton, Geometric control of universal hydrodynamic flow in a two-dimensional electron fluid, Phys. Rev. X **11**, 031030 (2021).

[5] E. M. Tennyson, T. A. S. Doherty, and S. D. Stranks, Heterogeneity at multiple length scales in halide perovskite semiconductors, Nat. Rev. Mater. **4**, 573 (2019).

[6] E. E. Fullerton, D. M. Kelly, J. Guimpel, I. K. Schuller, and Y. Bruynseraede, Roughness and giant magnetoresistance in Fe/Cr superlattices, Phys. Rev. Lett. **68**, 859 (1992).

[7] Z. Liang, K. Sasikumar, and P. Keblinski, Thermal transport across a substrate-thin-film interface: Effects of film thickness and surface roughness, Phys. Rev. Lett. **113**, 065901 (2014).

[8] Q. Song, J. Zhou, and G. Chen, Significant reduction in semiconductor interface resistance via interfacial atomic mixing, Phys. Rev. B **105**, 195306 (2022).

[9] A. I. Hochbaum, R. Chen, R. D. Delgado, W. Liang, E. C. Garnett, M. Najarian, A. Majumdar, and P. Yang, Enhanced thermoelectric performance of rough silicon nanowires, Nature **451**, 163 (2008).

[10] X. Qian, J. Zhou, and G. Chen, Phonon-engineered extreme thermal conductivity materials, Nat. Mater. **20**, 1188 (2021).

[11] T. Oyake, L. Feng, T. Shiga, M. Isogawa, Y. Nakamura, and J. Shiomi, Ultimate confinement of phonon propagation in silicon nanocrystalline structure, Phys. Rev. Lett. **120**, 045901 (2018).

[12] M. Rahbar, B. Li, N. Hunter, I. Al Keyyam, T. Wang, E. Shi, and X. Wang, Observing grain boundary-induced phonons mean free path in highly aligned SWCNT bundles by low-momentum phonon scattering, Cell Rep. Phys. Sci. **4**, 101688 (2023).

[13] M. N. Luckyanova, J. Garg, K. Esfarjani, A. Jandl, M. T. Bulsara, A. J. Schmidt, A. J. Minnich, S. Chen, M. S. Dresselhaus, Z. Ren, E. A. Fitzgerald, and G. Chen, Coherent phonon heat conduction in superlattices, Science **338**, 936 (2012).

[14] J. Ravichandran, A. K. Yadav, R. Cheaito, P. B. Rossen, A. Soukiassian, S. J. Suresha, J. C. Duda, B. M. Foley, C.-H. Lee, Y. Zhu, A. W. Lichtenberger, J. E. Moore, D. A. Muller, D. G. Schlom, P. E. Hopkins, A. Majumdar, R. Ramesh, and M. A. Zurbuchen, Crossover from incoherent to coherent phonon scattering in epitaxial oxide superlattices, Nat. Mater. **13**, 168 (2014).

[15] S. Xiong, K. Sääskilahti, Y. A. Kosevich, H. Han, D. Donadio, and S. Volz, Blocking phonon transport by structural resonances in alloy-based nanophononic metamaterials leads to ultralow thermal conductivity, Phys. Rev. Lett. **117**, 025503 (2016).

[16] T. Juntunen, O. Vänskä, and I. Tittonen, Anderson localization quenches thermal transport in aperiodic superlattices, Phys. Rev. Lett. **122**, 105901 (2019).

[17] S. Michele, M. Nicola, and M. Francesco, Unified theory of thermal transport in crystals and glasses, Nat. Phys. **15**, 809 (2019).

[18] D. Ma, A. Arora, S. Deng, G. Xie, J. Shiomi, and N. Yang, Quantifying phonon particle and wave transport in silicon nanophononic metamaterial with cross junction, Mater. Today Phys. **8**, 56 (2019).

[19] M. I. Hussein, C.-N. Tsai, and H. Honarvar, Thermal conductivity reduction in a nanophononic metamaterial versus a nanophononic crystal: A review and comparative analysis, Adv. Funct. Mater. **30**, 1906718 (2020).

[20] M. N. Luckyanova, J. Mendoza, H. Lu, B. Song, S. Huang, J. Zhou, M. Li, Y. Dong, H. Zhou, J. Garlow, L. Wu, B. J. Kirby, A. J. Grutter, A. A. Puretzky, Y. Zhu, M. S. Dresselhaus, A. Gossard, and G. Chen, Phonon localization in heat conduction, Sci. Adv. **4**, eaat9460 (2018).

[21] J. Zhang, H. Zhang, J. Wu, X. Qian, B. Song, C.-T. Lin, T.-H. Liu, and R. Yang, Vacancy-induced phonon localization in boron arsenide using a unified neural network interatomic potential, Cell Rep. Phys. Sci. **5**, 101760 (2024).

[22] A. Fiorentino, E. Drigo, S. Baroni, and P. Pegolo, Unearthing the foundational role of anharmonicity in heat transport in glasses, arXiv:2307.09370.

[23] Z. Zhang, Y. Guo, M. Bescond, J. Chen, M. Nomura, and S. Volz, Heat conduction theory including phonon coherence, Phys. Rev. Lett. **128**, 015901 (2022).

[24] Y. Cheng, Z. Fan, T. Zhang, M. Nomura, S. Volz, G. Zhu, B. Li, and S. Xiong, Magic angle in thermal conductivity of twisted bilayer graphene, Mater. Today Phys. **35**, 101093 (2023).

[25] R. Chen, A. I. Hochbaum, P. Murphy, J. Moore, P. Yang, and A. Majumdar, Thermal conductance of thin silicon nanowires, Phys. Rev. Lett. **101**, 105501 (2008).

[26] J. Lim, K. Hippalgaonkar, S. C. Andrews, A. Majumdar, and P. Yang, Quantifying surface roughness effects on phonon transport in silicon nanowires, Nano Lett. **12**, 2475 (2012).

[27] P. Martin, Z. Aksamija, E. Pop, and U. Ravaioli, Impact of phonon-surface roughness scattering on thermal conductivity of thin Si nanowires, Phys. Rev. Lett. **102**, 125503 (2009).

[28] J. Carrete, L. J. Gallego, L. M. Varela, and N. Mingo, Surface roughness and thermal conductivity of semiconductor nanowires: Going below the Casimir limit, Phys. Rev. B **84**, 075403 (2011).

[29] N. K. Ravichandran, H. Zhang, and A. J. Minnich, Spectrally resolved specular reflections of thermal phonons from atomically rough surfaces, Phys. Rev. X **8**, 041004 (2018).

[30] H. Qiao, E. Dumur, G. Andersson, H. Yan, M. Chou, J. Grebel, C. R. Conner, Y. J. Joshi, J. M. Miller, R.

G. Povey, X. Wu, and A. N. Cleland, Splitting phonons: Building a platform for linear mechanical quantum computing, Science **380**, 1030 (2023).
[31] M. Maldovan, Phonon wave interference and thermal bandgap materials, Nat. Mater. **14**, 667 (2015).
[32] H. Chen, H. Wang, Y. Yang, N. Li, and L. Zhang, Rough boundary effect in thermal transport: A Lorentz gas model, Phys. Rev. E **98**, 032131 (2018).
[33] F. Tian *et al.*, Unusual high thermal conductivity in boron arsenide bulk crystals, Science **361**, 582 (2018).
[34] W. Niu, J. Ma, and X. Feng, Precise structural regulation and band-gap engineering of curved graphene nanoribbons, Acc. Chem. Res. **55**, 3322 (2022).
[35] P. Ruffieux, S. Wang, B. Yang, C. Sánchez-Sánchez, J. Liu, T. Dienel, L. Talirz, P. Shinde, C. A. Pignedoli, D. Passerone, T. Dumslaff, X. Feng, K. Müllen, and R. Fasel, On-surface synthesis of graphene nanoribbons with zigzag edge topology, Nature **531**, 489 (2016).
[36] S. G. Volz and G. Chen, Molecular dynamics simulation of thermal conductivity of silicon nanowires, Appl. Phys. Lett. **75**, 2056 (1999).
[37] J. Chen, G. Zhang, and B. Li, Remarkable reduction of thermal conductivity in silicon nanotubes, Nano Lett. **10**, 3978 (2010).
[38] See Supplemental Material at http://link.aps.org/supplemental/10.1103/PhysRevApplied.21.064005 for the introduction of randomness, the effect of heat source (heat sink) length, the relationship between thermal conductivity and roughness at different widths, normalized thermal conductivity, the calculation details and figure of participation ratio and frequency-dependent thermal conductivity.
[39] S. Plimpton, Fast parallel algorithms for short-range molecular dynamics, J. Comput. Phys. **117**, 1 (1995).
[40] L. Lindsay and D. A. Broido, Optimized Tersoff and Brenner empirical potential parameters for lattice dynamics and phonon thermal transport in carbon nanotubes and graphene, Phys. Rev. B **81**, 205441 (2010).
[41] X. Wang, Z. Gao, G. Zhu, J. Ren, L. Hu, J. Sun, X. Ding, Y. Xia, and B. Li, Role of high-order anharmonicity and off-diagonal terms in thermal conductivity: A case study of multiphase $CsPbBr_3$, Phys. Rev. B **107**, 214308 (2023).
[42] Z. Zhang, Y. Ouyang, Y. Cheng, J. Chen, N. Li, and G. Zhang, Size-dependent phononic thermal transport in low-dimensional nanomaterials, Phys. Rep. **860**, 1 (2020).
[43] D. Ma, H. Ding, H. Meng, L. Feng, Y. Wu, J. Shiomi, and N. Yang, Nano-cross-junction effect on phonon transport in silicon nanowire cages, Phys. Rev. B **94**, 165434 (2016).
[44] J. D. Gale, GULP: A computer program for the symmetry-adapted simulation of solids, J. Chem. Soc., Faraday Trans. **93**, 629 (1997).
[45] A. Bodapati, P. K. Schelling, S. R. Phillpot, and P. Keblinski, Vibrations and thermal transport in nanocrystalline silicon, Phys. Rev. B **74**, 245207 (2006).
[46] P. B. Allen, J. L. Feldman, J. Fabian, and F. Wooten, Diffusons, locons and propagons: Character of atomic vibrations in amorphous Si, Philos. Mag. B **79**, 1715 (1999).
[47] D. Donadio and G. Galli, Atomistic simulations of heat transport in silicon nanowires, Phys. Rev. Lett. **102**, 195901 (2009).
[48] K. Sääskilahti, J. Oksanen, J. Tulkki, and S. Volz, Spectral mapping of heat transfer mechanisms at liquid-solid interfaces, Phys. Rev. E **93**, 052141 (2016).
[49] S. Tian, T. Wu, S. Hu, D. Ma, and L. Zhang, Boosting phonon transport across AlN/SiC interface by fast annealing amorphous layers, Appl. Phys. Lett. **124**, 042202 (2024).
[50] S. Hu, Z. Zhang, P. Jiang, J. Chen, S. Volz, M. Nomura, and B. Li, Randomness-induced phonon localization in graphene heat conduction, J. Phys. Chem. Lett. **9**, 3959 (2018).
[51] J. Maire, R. Anufriev, R. Yanagisawa, A. Ramiere, S. Volz, and M. Nomura, Heat conduction tuning by wave nature of phonons, Sci. Adv. **3**, e1700027 (2017).
[52] A. Kınacı, J. B. Haskins, C. Sevik, and T. Çağın, Thermal conductivity of BN-C nanostructures, Phys. Rev. B **86**, 115410 (2012).
[53] S. Park and R. S. Ruoff, Chemical methods for the production of graphenes, Nat. Nanotechnol. **4**, 217 (2009).

Correction: Missing and misplaced information in the Acknowledgment section has been rectified.